Transfer hydrogenation over sodium-modified ceria: enrichment of redox sites active for alcohol dehydrogenation

Nicholas C. Nelson,[a,b] *Brett W. Boote,*[a,b] *Pranjali Naik,*[a,b] *Aaron J. Rossini,*[a,b] *Emily A. Smith,*[a,b] *Igor I. Slowing*[a,b,]*

[a]US DOE Ames Laboratory, Ames, Iowa 50011, United States
[b]Department of Chemistry, Iowa State University, Ames, Iowa 50011, United States

*Corresponding author, E-mail address: islowing@iastate.edu

Abstract

Ceria (CeO_2) and sodium-modified ceria (Ce-Na) were prepared through combustion synthesis. Palladium was deposited onto the supports (Pd/CeO_2 and Pd/Ce-Na) and their activity for the aqueous-phase transfer hydrogenation of phenol using 2-propanol under liquid flow conditions was studied. Pd/Ce-Na showed a marked increase (6x) in transfer hydrogenation activity over Pd/CeO_2. Material characterization indicated water-stable sodium species were not doped into the ceria lattice, but rather existed as sub-surface carbonates. Modification of ceria by sodium provided more adsorption and redox active sites (i.e. defects) for 2-propanol dehydrogenation. This effect was an intrinsic property of the Ce-Na support and independent of Pd. The redox sites active for 2-propanol dehydrogenation were thermodynamically equivalent on both supports/catalysts. At high phenol concentrations, the reaction was limited by 2-propanol adsorption. Thus, the difference in catalytic activity was attributed to the different number of 2-propanol adsorption and redox active sites on each catalyst.

Keywords

Transfer hydrogenation, ceria, sodium, alcohol dehydrogenation, redox, defect sites, oxidation, flow chemistry

1. Introduction

The inevitable depletion of fossil fuels and the controversy that surrounds their use makes it imperative to develop sustainable, economical, and efficient alternatives to petrochemicals. Plant biomass is the most recognized alternative and is widely regarded as the most promising renewable resource to replace petroleum feedstocks.[1] Of plant biomass, lignin is the only large-scale source of aromatics. As such, there has been a significant amount of effort devoted and progress made to efficiently harvest the aromatics in a cost-competitive manner.[2] The obvious and urgent needs for more sustainable chemical processes will likely lead to the development of lignin-based technologies and allow it to become a significant source of renewable aromatics.[3] However, to take full advantage of renewable aromatic feedstocks, sustainable and economical downstream processes that convert the depolymerization products into high-value commodity chemicals need to be developed.[4]

Lignin is a phenolic-based polymer and therefore a significant portion of the depolymerization products are phenolics.[5, 6] Phenol finds its major use as a precursor for plastics often by reaction with other compounds or molecules. For example, phenol can be reduced to afford cyclohexanone and/or cyclohexanol. The ketone (K) and alcohol (A) products, either separately or in a mixture (KA oil), are predominantly used as precursors for nylon.[7] Industrial processes that convert phenol to precursors used in nylon production rely on high pressure molecular hydrogen as the reductant.[8] Therefore, it is advantageous to develop catalysts and catalytic systems that lower the hydrogen pressure needed for phenol reduction or eliminate the need for molecular hydrogen all together. Recently, there have been several catalytic systems developed for phenol reduction at or near atmospheric hydrogen pressures.[9] Far fewer systems have been developed that eliminate the need for molecular hydrogen through transfer hydrogenation.[10-

13] Thus, there is a present and forecasted need to develop catalytic transfer hydrogenation systems that can transform biomass platform molecules into high-value commodity chemical precursors and lessen our reliance on petroleum-based feedstocks for downstream processing of biomolecules.

In recent years there has been a surge in the development of heterogeneous transfer hydrogenation catalytic systems.[14] Oftentimes, these systems contain two components: one to activate the donor molecule for hydrogen liberation and the other to activate the liberated hydrogen for reduction of the unsaturated functionality. Noble metals are widely used to promote the latter, while homogenous inorganic or organic bases (e.g. NaOH, K-O^{t}Bu) have traditionally been used for the former. From an advanced catalyst design standpoint, it is beneficial to incorporate the necessary promoters within the solid catalyst to achieve the desired activity and avoid the undesired homogeneous components. In a previous study, we showed that ceria supported palladium was active for room temperature phenol hydrogenation with molecular hydrogen at atmospheric pressure.[15] Ceria is a mildly basic, redox active metal oxide and as such, a seemingly good candidate for transfer hydrogenation reactions. Considering its potential, ceria has been poorly studied for transfer hydrogenation catalysis. Catalytic systems involving iridium oxide,[16] gold,[17, 18] and nickel[19] supported on ceria have been reported for transfer hydrogenation of ketones and aldehydes without the use of a base promoter. Shimizu et al.[19] studied the transfer hydrogenation of ketones over Ni/CeO_2 catalyst using 2-propanol as the hydrogen donor. The catalyst showed good activity for aromatic and aliphatic ketone reduction. Although a base metal was used, the catalyst was not stable in air and thermal regenerative treatments were needed between recycling experiments.

Ceria and ceria-based materials are best known for their redox properties, which are related to the number and type of oxygen vacancies within the material.[20-31] The significant effort and progress made to understand the role of oxygen vacancies during catalytic processes has enabled the design of defect-engineered ceria-based materials.[32-38] Perhaps most notable are ceria materials with well-defined shapes that expose specific crystallographic planes, which dictate the amount and type of defect sites present.[39-43] The redox properties of these materials are oftentimes probed with short-chain alcohols, whose adsorption, reactions, and product distribution/desorption temperature are believed to depend on the defect sites present.[44-48] Typically, the more defect-rich ceria materials give rise to higher yields of dehydrogenation products. With this in mind, the development of ceria-based materials with high concentrations of defect sites should translate into high dehydrogenation activities and therefore be excellent candidates for transfer hydrogenation reactions. Herein, we report the combustion synthesis of ceria and sodium-modified ceria using cerium nitrate and cerium/sodium nitrate precursors, respectively. Sodium modification was found to increase the number of redox active sites on the surface that lead to 2-propanol dehydrogenation. Palladium was supported on both materials and their activity for phenol transfer hydrogenation using potentially renewable 2-propanol[49] is reported. Keeping along the lines of sustainable biomass upgrading, the reactions were run in liquid flow mode, which has the added advantages of high throughput and catalyst recycling efficiency.[50]

2. Results and discussion

2.1 Catalysis

Ceria (CeO_2) and the cerium-sodium oxide material (Ce-Na) with nominal 20 at. % Na loading were prepared using a modified solution combustion synthesis (SCS) with Pluronic polymer as fuel and metal nitrate salts. The SCS method was chosen due to its precedence for forming homogeneous multi-metal oxide composites.[51] Palladium was deposited onto Ce-Na (Pd/Ce-Na) and CeO_2 (Pd/CeO_2) through impregnation with palladium(II) acetate, followed by oxidative and reductive thermal treatments at 350 °C. The physicochemical properties of the as-synthesized supports and catalyst are summarized in Table S1.

The liquid flow transfer hydrogenation of phenol using 2-propanol as the sacrificial hydrogen donor with Pd/Ce-Na and Pd/CeO_2 catalysts proceeded through the formation of cyclohexanone and cyclohexanol in various proportions depending on reaction conditions (Table 1). Both catalysts displayed outstanding stability during 7-day continuous catalytic runs (Fig. 1a). However, Pd/Ce-Na showed a marked increase in transfer hydrogenation activity over Pd/CeO_2. For instance, under the conditions given in Table 1 for Entries 2 and 7, the rate of phenol conversion was nearly five times higher over Pd/Ce-Na than Pd/CeO_2 and about six times as high for Entries 5 and 10. As evident from Table 1, Pd/Ce-Na showed higher phenol conversion rates under all the reaction conditions tested. Both catalysts showed initial deactivation attributed to decreased surface area and/or Pd dispersion with TOS (Table S2). Pd/CeO_2 showed a higher initial deactivation than Pd/Ce-Na likely owing to operation of the latter near equilibrium conversion (83 % conversion) and better catalyst stability (Table S2). For Pd/Ce-Na, the ketone to alcohol yield ratio (K:A) varied from about 10:90 to 40:60 through control of the flow rate and phenol concentration (Table 1, Entries 1-5). The ketone yield was more or less constant when

varying these parameters, while the alcohol yield was more sensitive to these variations (Table 1, Entries 1-5). For Pd/CeO_2, the K:A ratio was larger than for Pd/Ce-Na, giving almost exclusively the ketone (Table 1, Entries 6-10). Both catalysts showed a higher conversion rate as the 2-propanol-water ratio was increased. Interestingly, neat 2-propanol resulted in a monotonic, yet significant decrease of conversion rate as a function of time over both catalysts which was not observed in the presence of water (Fig. S1). Washing the catalysts with water overnight at 140 °C after the reaction in neat 2-propanol resulted in regeneration of the original activity. This suggests the decreased activity may be related to hydroxyl disproportionation, which results in the removal of lattice oxygen through water formation.[52-55] In absence of water, the hydroxyl disproportionation equilibrium lies to the right in Scheme S1, giving oxygen deficient ceria, which is a poor oxidation catalyst.[52] The regeneration data implies that water is able to dissociatively adsorb on partially reduced ceria,[55-57] and shift the equilibrium in Scheme S1 to the left. Thus, water appears to be a necessary component to maintain hydroxyl disproportionation equilibrium in a way that favors the redox process. Arrhenius plots were constructed for [phenol] = 0.1 M and the apparent activation barriers for phenol conversion over Pd/CeO_2 and Pd/Ce-Na were 115 ± 3 kJ mol^{-1} and 48 ± 2 kJ mol^{-1}, respectively (Fig. 1b).

Table 1. Reaction conditions and catalytic results for transfer hydrogenation of phenol with 2-propanol.[a]

Entry	Catalyst	Phenol (M)	Flow Rate (μL min^{-1})	Conversion Rate (μmol g^{-1} h^{-1})	Yield (%)		K:A
					C=O	C-OH	
1	Pd/Ce-Na	0.150	44.1[b]	759 ± 6	13 ± 1	82 ± 1	14:86
2	Pd/Ce-Na	0.150	95.6[c]	1390 ± 40	26 ± 1	54 ± 2	33:67
3	Pd/Ce-Na	0.150	191[d]	1410 ± 20	16 ± 1	25 ± 1	40:60
4	Pd/Ce-Na	0.200	44.1	905 ± 16	19 ± 1	67 ± 2	22:78
5	Pd/Ce-Na	0.200	95.6	1360 ± 60	18 ± 1	41 ± 3	30:70
6	Pd/CeO_2	0.150	44.1	266 ± 9	31 ± 4	2 ± 1	93:7
7	Pd/CeO_2	0.150	95.6	287 ± 8	16 ± 1	<1	96:4
8	Pd/CeO_2	0.150	191	279 ± 3	8 ± 1	0	100:0
9	Pd/CeO_2	0.200	44.1	215 ± 4	20 ± 2	<1	97:3
10	Pd/CeO_2	0.200	95.6	217 ± 5	10 ± 2	0	100:0

[a]0.5g of catalyst was used for all reactions. Water was flowed over the catalyst at room temperature for 2 h before beginning the initial run (Entries 1, 6). After that, the reactions were run sequentially (Entries 2-5, 7-10). 90 v/v % aqueous 2-propanol was used for all reactions. Column temperature was 140 °C. Catalyst bed volume (V_{bed}) was 0.4 mL. Errors are reported as one standard deviation away from the mean. [b]For a flow rate of ~0.05 mL min^{-1}, 72 mL of reagent was used with 12 mL sample composite intervals generating 6 data points over 24 h. [c]For a flow rate of ~0.10 mL min^{-1}, 144 mL of reagent was used with 24 mL sample composite intervals generating 6 data points over 24 h. [d]For a flow rate of ~0.20 mL min^{-1}, 168 mL of reagent was used with 24 mL sample composite intervals generating 7 data points over 14 h.

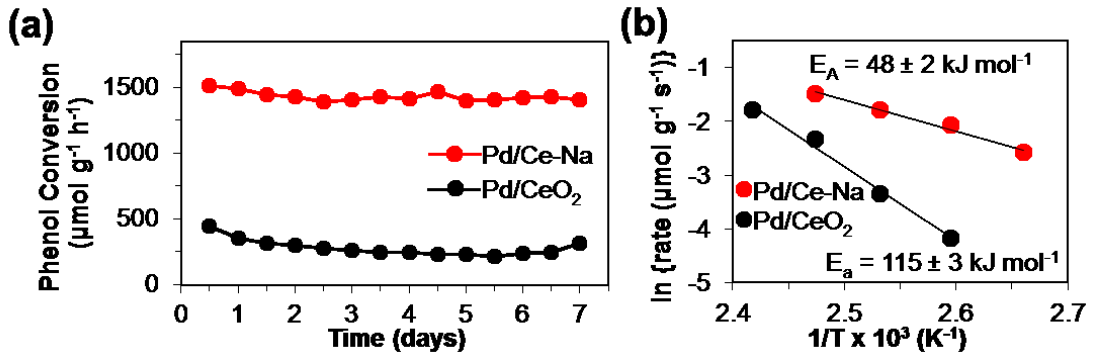

Fig. 1. (a) Phenol conversion rate for Pd/CeO_2 and Pd/Ce-Na during 7 day time-on-stream (TOS) study. Conditions: 0.15 M phenol in 90 v/v % aqueous 2-propanol, 0.5 g catalyst, ~0.1 mL min^{-1}, T = 140 °C, V_{bed} = 0.4 mL. Each data point corresponds to 72 mL product stream composite. (b) Arrhenius plots of phenol conversion over Pd/CeO_2 (E_A = 115 kJ mol^{-1}) and Pd/Ce-Na (E_A = 48

175 kJ mol^{-1}). Conditions: 0.1 M phenol in 90 v/v % aqueous 2-propanol, 0.5 g catalyst, ~0.1 mL
176 min^{-1}, V_{bed} = 0.4 mL. Each data point (at each temperature) corresponds to the average of 6 rate
177 measurements collected at 4 h sampling intervals (24 mL composite) over 24 h.

178 Physicochemical properties are often invoked to explain differences in activity and were found
179 to be similar for both catalysts after the reaction (Table S3). That is, the specific surface area of
180 Pd/CeO_2 decreased by an order of magnitude over the course of the reaction, which made it
181 comparable to Pd/Ce-Na. Likewise, the Pd dispersion value on both catalysts decreased to about
182 10 % during time-on-stream, suggesting Na does not enhance Pd dispersion.[58, 59] Both
183 catalysts showed the same Pd loadings before and after reaction, which is consistent with the
184 long-term catalyst stability. The similar post-reaction physicochemical properties between the
185 catalysts suggest that sodium modification was able to promote transfer hydrogenation activity.
186 In order to understand the role of sodium promotion more clearly, preferential attention was
187 given to support characterization. The role of palladium was studied where deemed relevant.

188 *2.2 Materials Characterization*

189 Elemental analysis of as-synthesized Ce-Na support confirmed sodium was present at 18 at. %
190 and agreed well with nominal loading of 20 at. % (Table 2, Entry 1). DRIFT (Fig. S2-S4) and
191 XPS (Fig. S5) analysis showed sodium was present as a carbonate. ICP analysis of Ce-Na after
192 continuous-flow aqueous treatment at room temperature for twelve hours showed a drastic
193 reduction of sodium content from 18 to 4.0 at. % (Table 2, Entries 1, 3), with most soluble
194 sodium species removed after two hours during washing (Fig. S6). The data presented in Fig. S6
195 was obtained after washing the material at catalytic temperatures (i.e. 140 °C) and showed a
196 further decrease in sodium loading to 2.6 at. % (Table 2, Entry 4). Quite surprisingly, sodium
197 was retained even after 7 days on stream (Table 2, Entry 5). While ICP analysis confirmed the

presence of sodium after washing, XPS (Fig. S5g) indicated that there were minimal amounts of sodium on the surface, suggesting that sodium species are contained within the material. Bearing in mind the aqueous conditions used during catalysis, all Ce-Na and Pd/Ce-Na characterization was performed after aqueous washing at room temperature (Table 2, Entry 3).

Table 2. Physicochemical properties of supports and catalysts under varying conditions.

Entry	Sample	Surface Area (m^2 g^{-1})[a]	Na Loading (at. %)[b]	Lattice Constant (Å)[c]
1	Ce-Na	29	18 ± 1[d]	5.412
2	CeO_2	210	0	5.412
3	Ce-Na[e]	42	4.0 ± 0.2[f]	5.412
4	Ce-Na[g]	40	2.6 ± 0.1[h]	---
5	Pd/Ce-Na[i]	20	2.7 ± 0.2[j]	---

[a]Determined by nitrogen physisorption using BET approximation. [b]Determined by ICP-OES and is relative to Ce. [c]Determined using HighScore software. [d]Measured across three batches. [e]Washed with flowing water (0.1 mL min^{-1}) for 12 h at room temperature. [f]Measured across two batches with two sample preps in duplicate (i.e. 8 data points). [g]Washed with flowing water (0.1 mL min^{-1}) for 12 h at 140 °C. [h]Measured for one batch with two sample preparations in duplicate (i.e. 4 data points). [i]Results after 7 d reaction. [j]Measured in duplicate with two sample preparations (i.e. 4 data points).

The PXRD pattern of the supports (Fig. 2a) and catalysts (Fig. S7) exhibited diffraction peaks that could be indexed to the fluorite structure of ceria, with no other reflections observed. The absence of sodium-containing reflections (e.g. Na_2O, Na_2CO_3, etc.) in the diffraction pattern suggests sodium species could be amorphous or have a crystallite size below the detection limit of the instrument. Since XPS analysis indicated that sodium was not present on or near the surface, it is also possible that sodium was doped into the ceria matrix. Rietveld analysis showed no significant difference in lattice constant between Ce-Na and CeO_2 (Table 2, Entries 1-3). The

identical lattice constants between Ce-Na and CeO_2 could be an indication that residual sodium species were not contained within the bulk ceria lattice. Alternatively, it could reflect the similar sizes of Ce^{4+} (0.97 Å)[60] and Na^{+} (0.99 Å)[60], which has been observed for Pr- (0.99 Å)[60] doped ceria.[61, 62]. The identical lattice parameters from PXRD analysis were also supported by HR-TEM imaging for several crystallites of Ce-Na that gave an average d-spacing of 0.31 ± 0.03 nm (Fig. S8). This value corresponds to the (111) surface termination and is also the predominant facet observed for CeO_2 (Fig. S9).[15] The result rules out structural promotion (i.e. surface termination) for the higher rate of phenol turnover and lower activation barrier for conversion.

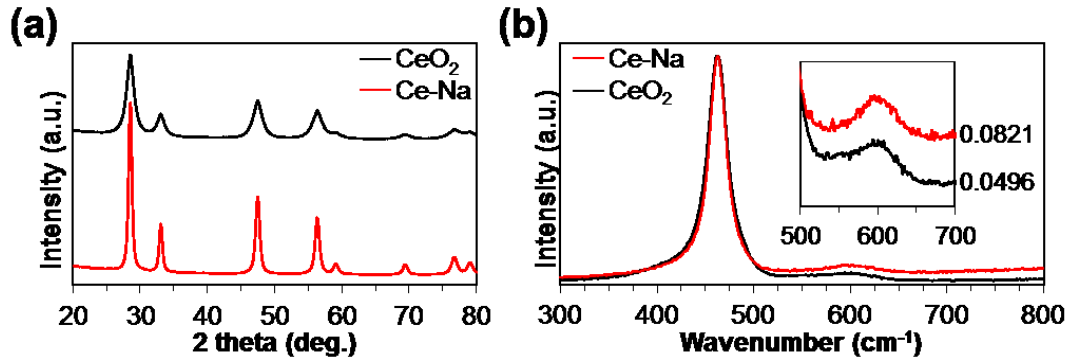

Fig. 2. (a) PXRD patterns for CeO_2 and Ce-Na showing cubic fluorite phase. (b) Raman spectra using 488 nm excitation for CeO_2 and Ce-Na. Inset shows band associated with intrinsic defects (D-band). The numbers represent the ratio (A_D:A_{F2g}) of the peak areas for the D-band (600 cm^{-1}) and the F_{2g}-band (462 cm^{-1}).

Given the comparable size of sodium and cerium (IV) cations, PXRD may not be suitable for determining whether sodium was doped into the ceria lattice. In direct contrast to PXRD, which primarily gives information related to the cationic sublattice, Raman spectra of fluorite-type oxides are sensitive to bulk oxygen lattice vibrations, which are related to M-O bond symmetry and defects. The Raman spectra for CeO_2 and Ce-Na are shown in Fig. 2b. Both samples

exhibited Raman bands around 462 cm^{-1} and were attributed to the F_{2g} triply degenerate Raman-active phonon of the cubic CeO_2-fluorite phase.[41, 63, 64] This band can be viewed as a symmetrical stretching vibration of the oxygen atoms surrounding a cerium cation (i.e. CeO_8). Thus, the location of the band is sensitive to the M-O bond lengths and symmetry present in ceria-based materials.[62, 64] The band positions for the two materials were identical suggesting similar bond lengths in accordance with the lattice constants obtained from PXRD analysis. Both samples also exhibited bands around 600 cm^{-1} that have been suggested to result from the presence of intrinsic oxygen defects.[41] The ratio between the defect band (D-band) and the F_{2g} band (i.e. A_D:A_{F2g}) is used to compare the amounts of intrinsic defects between different ceria-based materials.[41, 65] Ce-Na showed a higher A_D:A_{F2g} ratio (1.7×) indicating more defects compared to CeO_2 even with the former having a larger crystallite size.[64] However, the exact nature of these defects, either vacancy-interstitial (Frenkel) or Ce^{3+} substitutional in an octahedral environment, is still debated.[41, 63] Another defect band around 570 cm^{-1} has been observed for ceria during thermal treatment under reducing environments and is attributed to oxygen vacancies formed during reduction (i.e. extrinsic oxygen vacancies).[44] The same band has also been observed upon substitutional doping of cerium cations with aliovalent metals and is thought to result from charge compensation and is thus associated with extrinsic oxygen vacancies.[62] The absence of this band in Ce-Na suggests sodium is not acting as a substitutional dopant that exhibits charge-compensation. Charge compensation through formation of Na^+-Ce^{3+} cationic pairs could also be possible and would not involve formation of oxygen vacancies. However, this motif would be expected to result in differences of lattice constant between the two materials due to the larger ionic radius of Ce^{3+}, which was not

observed in PXRD analysis. Thus, the PXRD and Raman data together suggest sodium was not acting as a dopant.

Structural analysis of the Ce-Na support indicated that sodium was not contained within the ceria lattice, but it was shown through chemical analysis that sodium species are still present even after washing with water at elevated temperatures for extended periods of time (Table 2). Considering that the predominant sodium species before washing were carbonates, the residual sodium may be in the form of carbonates that are trapped at the grain boundaries within the bulk of the particles (Table S1, Fig. S8). Fig. S10 shows the CO_2-TPD profile while monitoring the heat flow and weight loss for the Ce-Na support. The TGA-DSC-MS analysis showed two high temperature CO_2 desorption peaks around 700-800 °C and 900-1100 °C. The former CO_2 desorption peak was exothermic while the latter was endothermic. The exothermic transition with evolution of CO_2 suggests carbonate decomposition and likely arises from sodium carbonate decay. Anhydrous sodium carbonate is known to decompose at temperatures higher than 800 °C, but metal oxide additives have been shown to lower the decomposition temperature.[66] Furthermore, the decomposition of sodium carbonate is an exothermic process in agreement with the thermal data and is expected to result in the formation of sodium oxide. The endothermic CO_2 evolution peak could be due to CO_2 desorbing from sodium oxide. The total weight loss from the onset of the exothermic transition to the end of the endothermic transition (i.e. 700-1100 °C), assuming sodium carbonate decomposition, allowed an estimation of residual sodium to be 3.8 at. %. This result is in excellent agreement with that obtained from elemental analysis (Table 2, Entry 3). Furthermore, XPS depth-profiling experiments showed the Na 1s binding energy was characteristic of sodium carbonate (Fig. S11).[67] Thus, it appears that

the insoluble sodium fraction was sodium carbonate and that it was largely inaccessible to water (Table 2).

^{23}Na solid-state NMR (SSNMR) spectroscopy was also performed on the Ce-Na support. ^{23}Na is a 100% naturally abundant $I = 3/2$ quadrupolar nucleus which normally gives rise to relatively narrow solid-state NMR spectra. The ^{23}Na spin echo SSNMR spectrum of Ce-Na support possessed a relatively broad, featureless resonance (Fig. S12A). A 2D triple quantum multiple quantum magic angle spinning (MQMAS) experiment suggested that the broadening of the ^{23}Na SSNMR spectrum was primarily due to a distribution of isotropic ^{23}Na chemical shifts in the range of 10 to –10 ppm; broadening from the second order quadrupolar interaction was minimal (Fig. S12A). This suggests that there are many distinct sodium sites/environments, and within these sites the sodium ions must reside at sites of relatively high spherical symmetry (i.e., pseudo-octahedral coordination environments). A ^{23}Na{^{1}H} rotational echo double resonance (REDOR) experiment was performed to assess the spatial proximity of the Na ions to protons. The REDOR experiment indicates that ca. 60% of the Na ions are proximate (within 5 Å) of ^{1}H nuclei (Fig. S12B and Fig. S12C). This would suggest that the majority of the sodium carbonate is present as a hydrated phase or nearby to sorbed water. This is perhaps to be expected since the Ce-Na support was thoroughly washed to remove excess Na. Several distinct crystalline anhydrous and hydrated sodium carbonate phases have previously been reported.[68, 69] Therefore, the range of isotropic ^{23}Na chemical shifts most likely arises from the presence of a variety of hydrated and anhydrous sodium carbonate phases/environments. Keeping the XPS results in mind, these sodium carbonate phases are likely trapped in between the ceria grains.

The role of residual sodium carbonate during catalysis remains unclear. The insolubility under aqueous conditions at elevated temperatures for 7 days suggests that it is not accessible to the

environment and thus should not participate directly in the catalysis. To better understand the role of sodium carbonate a control sample was prepared through impregnation of CeO_2 with aqueous $NaNO_3$ (20 at. %) followed by calcination at 450 °C (Na/CeO_2). Pd was then deposited on the support ($Pd/Na/CeO_2$). It is expected that decomposition of the sodium precursor should yield surface sodium carbonate species that are easily removed with water and thus clarify the role of sodium carbonate. Quite remarkably, the control catalyst was slightly more active than Pd/Ce-Na (Fig. S13). ICP analysis revealed that $Pd/Na/CeO_2$ contained 1.1 Na-at. % after reaction, which is about a 60 % decrease of Na content compared to Pd/Ce-Na (Table 2, Entry 5). XPS depth profiling experiments showed the Na 1s binding energy for Na/CeO_2 (washed with water at room temperature) was consistent with sodium carbonate (Fig. S14). The result suggests that the physical amount of sodium carbonate during catalysis does not affect activity, at least from about 1-3 Na-at. %. Although the results provide some insight into the role of sodium carbonate, they are not conclusive.

Considering that bulk characterization techniques did not support the formation of sodium-doped ceria and that the physical amount of sodium carbonate doesn't appear to correlate with activity, it is possible that sodium modification affects the surface properties of the material. XPS analysis was conducted on both supports to probe possible electronic structure differences that could provide insight into the different catalytic activity. The Ce 3d spectral region (Fig. S15a) showed characteristic peaks attributed to Ce(IV),[70-73] with no obvious difference between the two supports. The O 1s spectral region shown in Fig. S15b displayed subtle differences between CeO_2 and Ce-Na. The O 1s spectrum peak maximum, assigned to lattice oxygen, shifted from 529.5 eV (CeO_2) to 529.3 eV (Ce-Na). The shift signifies, on average, a more electron-rich environment of lattice oxygens. Since sodium is present it would seem plausible that the

apparent increased oxygen electron density for Ce-Na could be due to higher material basicity, which has been observed for other metal oxides modified with sodium[74, 75] and could explain the different reaction rates observed. However, the basic properties and C-H activating ability[76] of the two materials were found to be identical by testing with basicity probes and base-catalyzed reactions (Fig. S16-S18, Table S4-S5). For completeness, the acidic properties were also found to be unmodified (Fig. S19-20). This data indicates that the acid-base properties for Ce-Na were unaltered relative to CeO_2 and that these reactivity descriptors are not relevant for the activity difference observed during phenol transfer hydrogenation.

2.3 Redox Properties and Kinetic Analysis

The most notable reactivity descriptor for ceria-based materials is the redox property. The redox property of ceria correlates to the number of defects within the material, especially as they relate to oxygen vacancies.[20, 35, 41, 42, 44, 77] Since 2-propanol oxidation is a prerequisite for phenol turnover, the 2-propanol reactivity over both CeO_2 and Ce-Na were studied. The temperature programmed surface reaction (TPSR) of 2-propanol was used to determine the relationship between acetone formation and the transfer hydrogenation activity of the two materials. At this point it should be noted that 2-propanol was adsorbed dissociatively[52, 78-80] on both materials as evidenced by two ν(C-O) stretching bands at 1162 and 1132 cm^{-1} corresponding to end-on and bridging coordination of isopropoxide to cerium cations, respectively (Fig. S21). The materials were saturated *ex situ* with 2-propanol and heated under Ar while monitoring evolved 2-propanol (m/z = 45), acetone (m/z = 43, 58), and propylene (m/z = 41). The characteristic acetone signal at m/z = 58, whose intensity is weak relative to the somewhat uncharacteristic signal at m/z = 43, was monitored to ensure the signal at m/z = 43 is primarily due to acetone desorption. The identical profiles observed for all samples at m/z = 43

and m/z = 58 indicates that the intensity of the m/z = 43 signal is primarily due to evolved acetone (Fig. S22). Fig. 3a, b shows the 2-propanol, acetone, and propylene signal intensity profile versus temperature for CeO_2 and Ce-Na, respectively. For CeO_2, acetone desorption occurred over a broad temperature range. Onset desorption occurred around 50 °C and continued to about 320 °C. There were two major desorption maxima centered at 133 °C and 237 °C, with a significant shoulder around 300 °C. Unreacted 2-propanol also desorbed over a broad temperature range spanning 50-275 °C, with two maxima observed at 105 °C and 208 °C slightly below the acetone maxima. A small propylene desorption was found at 307 °C. For Ce-Na, onset desorption also occurred around 50 °C with a dominant acetone desorption maximum at 150 °C and a significant shoulder at 228 °C. Unreacted 2-propanol desorbed over 50-250 °C with single maximum at 120 °C. There were negligible amounts of propylene observed.

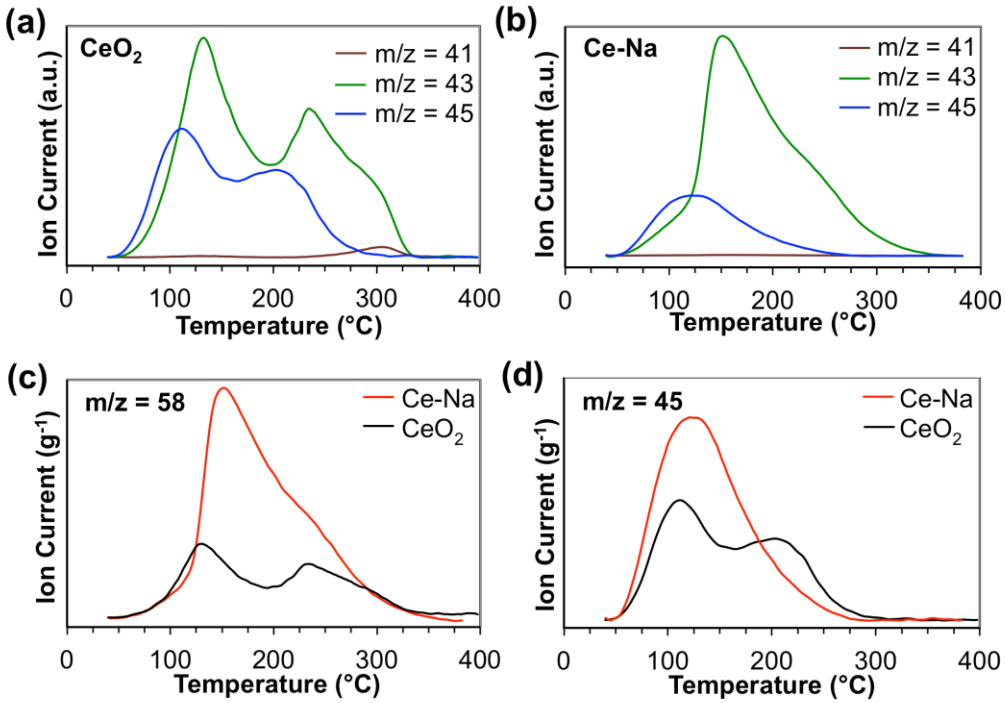

Fig. 3. TPD-MS profile for TPSR of adsorbed 2-propanol on (a) CeO_2 and (b) Ce-Na. The m/z =41, 43, and 45 signals correspond to propylene, acetone, and 2-propanol, respectively. Mass

365 normalized TPD-MS profile for TPSR of adsorbed 2-propanol on Ce-Na and CeO_2 while
366 monitoring (c) m/z = 58 and (d) m/z = 45 which correspond to acetone and 2-propanol,
367 respectively.

368 The signal corresponding to acetone (m/z = 58) for Ce-Na and CeO_2 were normalized to the
369 material mass and are shown in Fig. 3c. The formation rate of acetone is clearly higher on Ce-Na
370 indicated by the increased slope before the first maximum. Curiously, the temperature at
371 maximum acetone desorption were similar for Ce-Na and CeO_2. In addition, both materials
372 showed an acetone desorption shoulder around 240 °C. Typically, the desorption maximum is
373 proportional to the activation energy for the rate limiting step. This implies that the higher rate of
374 acetone formation observed for TPSR of 2-propanol on Ce-Na was not due to a reduced
375 activation barrier during an elementary reaction step. This result also indicates that the higher
376 rate can be attributed to more active sites present on the surface of Ce-Na in spite of the large
377 difference in surface area between the two materials. According to Redhead,[81, 82] the
378 activation energy of acetone formation on the two materials using the first desorption maximum
379 was 106 ± 21 kJ mol^{-1} and 101 ± 20 kJ mol^{-1} for Ce-Na and CeO_2, respectively. Considering that
380 formation of adsorbed isopropoxide occurs at room temperature (Fig. S21) and that acetone
381 shows little affinity for the surface of ceria above room temperature,[52] it seems likely the
382 observed activation barrier is due to C-H scission of adsorbed isopropoxide to form acetone. This
383 elementary reaction step is a redox process implying that there are more redox active centers on
384 Ce-Na and that these redox centers are equivalent. The relative areas of the mass-normalized
385 acetone TPD-MS profiles on the two supports showed 2.9× more acetone evolving from Ce-Na,
386 suggesting this support had about three times more 2-propanol dehydrogenation sites than CeO_2.

Additionally, the 2-propanol desorption profile for the two supports indicated a higher amount of desorbed 2-propanol on Ce-Na (Fig. 3d).

TPSR of adsorbed 2-propanol clearly showed the rate of acetone formation is higher for Ce-Na than for CeO_2, but the actual catalytic conditions are quite different and the reactant-limited TPSR results of the supports may not be representative during catalysis. Therefore, the rate of acetone formation under catalytic conditions was monitored by trapping with 2,4-dinitrophenylhydrazine and quantified using ^{1}H-NMR. The acetone formation rate was monitored at 140 °C under liquid flow conditions with 90 v/v % aqueous 2-propanol. For CeO_2 and Ce-Na the rates were 7 μmol g^{-1} h^{-1} and 13 μmol g^{-1} h^{-1}, respectively (Table 3, Entries 1, 2). For Pd/CeO_2 and Pd/Ce-Na, the average acetone formation rate observed over three trials was 2920 ± 80 μmol g^{-1} h^{-1} and 6270 ± 40 μmol g^{-1} h^{-1}, respectively (Table 3, Entries 3, 4). The increased 2-propanol dehydrogenation rate of both catalysts was likely due to the activity of Pd for 2-propanol dehydrogenation.[83] The TPSR study of adsorbed 2-propanol over the supports indicated the average acetone formation rate (i.e. from 40-400 °C) was about three times higher over Ce-Na, which was more than observed with the catalysts under catalytic conditions (2.1x). However, the TPSR study spanned a much broader temperature range than the catalytic study and is an average over each temperature within that range. Comparing the two y-maxima (130-150 °C) from the TPSR TPD-MS curve for evolved acetone (Fig. 3c) should indicate the relative dynamic acetone formation rate under reaction conditions (Table 3, Entries 3, 4). The relative maxima for evolved acetone between the two materials from TPSR of 2-propanol (2.4x) was in good agreement for the relative rates under dynamic liquid conditions using the catalysts (2.1x). Thus, given the acetone formation rates for the supports, it appears that palladium increases the acetone formation rate over both catalysts more or less equally, but the support largely dictates

the difference in the observed acetone formation rate. The similar 2-propanol dehydrogenation rate ratios between the supports and catalysts (Table 2, Entry 3 and 5, respectively) indicate that the amount of sodium species does not significantly affect dehydrogenation activity and that sodium carbonates are mere spectators in the reaction. This is also consistent with sodium species residing below the surface.

Table 3. Acetone formation rates over supports and catalysts in absence and presence of phenol.[a]

Entry	Catalyst	[Phenol] (M)	Acetone Rate (μmol g^{-1} h^{-1})	C=O Rate (μmol g^{-1} h^{-1})[b]	C-OH Rate (μmol g^{-1} h^{-1})[b]	Expected Acetone Rate (μmol g^{-1} h^{-1})[c]
1	CeO_2	0	7 ± 0.7[e]	---	---	---
2	Ce-Na	0	13 ± 1.3[e]	---	---	---
3	Pd/CeO_2	0	2920 ± 80[d]	---	---	---
4	Pd/Ce-Na	0	6270 ± 40[d]	---	---	---
5	Pd/CeO_2	0.15	576 ± 58[e]	288	12	612
6	Pd/Ce-Na	0.15	3680 ± 368[e]	476	974	3874

[a]Conditions: 90 v/v % aqueous 2-propanol, 0.5g of catalyst, 0.1 mL min^{-1}, T = 140 °C, V_{bed} = 0.4 mL. [b]Rates obtained from data found in Table 1, Entries 2, 7. [c]Calculated assuming 2 moles of acetone per mole of cyclohexanone and 3 moles of acetone per mole of cyclohexanol. [d]Average rate from three separate reactions. Errors represent one standard deviation from the mean. [e]Rate from one reaction. Errors represent average relative error determined during method validation (see experimental).

Although there was a clear enhancement in the rate of evolved acetone for Pd/Ce-Na, it did not represent the difference in phenol transfer hydrogenation rates observed (3-6x), which should correlate to the amount of acetone formed. To ensure that our assumption of a one-to-one acetone to molecular hydrogen stoichiometric relationship was valid, the amount of acetone formed during phenol transfer hydrogenation was measured under the conditions found in Table 1, Entries 2, 7. The evolved acetone for Pd/Ce-Na and Pd/CeO_2 were 3680 μmol g^{-1} h^{-1} and 576

μmol g^{-1} h^{-1}, respectively (Table 3, Entries 5, 6). These results agree well with the expected amount of acetone that should be formed considering the yield of products (Table 3).

A series of kinetic experiments were run to understand the cause of the lower activation barrier for Pd/Ce-Na (Fig. 1b) since 2-propanol TPSR suggests there should be no difference. The experimental data showed that the acetone formation rate over both catalysts decreased in presence of phenol, likely due to their affinity for the same adsorption sites.[15, 52] However, the relative percent decrease was much more severe over Pd/CeO_2 (80 %) than over Pd/Ce-Na (33 %) (Table 3). In addition, the difference between phenol conversion rates for the two catalysts increased with phenol concentration (Table 1). These results suggest the difference in apparent activation barrier may be related to the barrier for 2-propanol adsorption in the presence of phenol. Here, we are assuming that the surface kinetics follow Langmuir-Hinshelwood mechanism for competitive binding. That is, increasing the phenol concentration should lead to higher binding site occupancy, which would hinder 2-propanol adsorption and limit turnover. Evidence for this type of behavior was obtained by monitoring the phenol conversion rate as a function of phenol concentration (Fig. 4). Both materials showed a non-linear dependence of rate versus phenol concentration at conversions less than unity. The reaction rate profiles are characteristic for competitive adsorption.[82] The rate data also suggests there are more 2-propanol/phenol adsorption sites that lead to phenol turnover on Pd/Ce-Na shown by the up and rightward shift of the rate profile relative to Pd/CeO_2. That is, if the amount of 2-propanol/phenol adsorption sites were equal, the curve would be expected to shift straight up due to the increased number of redox active sites previously shown. This was supported through phenol adsorption isotherms that showed there were more phenol/2-propanol adsorption sites on the Ce-Na support even with the surface area of CeO_2 being five times greater (Fig. 5a). The y-intercept of the

linear region was taken as the approximate monolayer coverage and gave 77 μmol g^{-1} and 36 μmol g^{-1} for Ce-Na and CeO_2, respectively. This ratio (2.1) agrees well with the mass normalized area summation of all monitored reactants and products from the TPSR-MS profiles for Ce-Na and CeO_2 (2.4) (Fig. 3c, d). Furthermore, the ratio is identical to the ratio of acetone formation rates observed over the two catalysts in the absence of phenol (Table 3, Entries 3, 4). Although the latter comparison is made between the supports and catalysts, it does suggest that the phenol adsorption sites are the same as 2-propanol and that these adsorption sites are active for 2-propanol dehydrogenation.

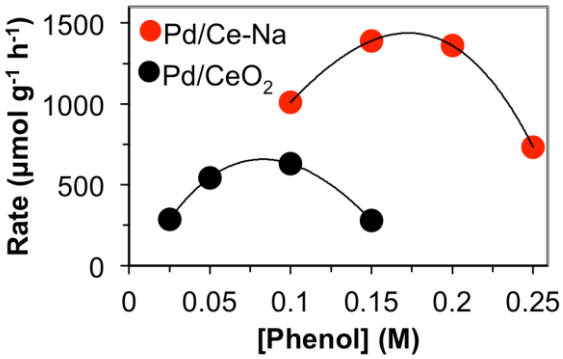

Fig. 4. Phenol conversion rate versus phenol concentration over Pd/CeO_2 and Pd/Ce-Na. Conditions: 90 v/v % aqueous 2-propanol, 0.5 g catalyst, ~0.1 mL min^{-1}, T = 140 °C, V_{bed} = 0.4 mL.

Further evidence for the apparent activation barrier arising from the barrier for 2-propanol adsorption in presence of phenol was obtained by monitoring the phenol conversion rate as a function of aqueous 2-propanol concentration. Under the reaction conditions shown in Fig. S23, the apparent order for 2-propanol during the transfer hydrogenation of phenol over Pd/CeO_2 and Pd/Ce-Na were 3.7 and 0.9, respectively. The dependence of phenol conversion rate on the 2-propanol concentration over both catalysts indicates that water competes for the same binding

sites as 2-propanol/phenol. The higher dependence of conversion rate on 2-propanol concentration for Pd/CeO_2 is consistent with phenol blocking a larger percentage of 2-propanol adsorption sites (i.e. Langmuir-Hinshelwood competitive binding) since all other conditions are equal. This was also made apparent by the drastic color change of CeO_2 in the presence of a 2-propanol/phenol solution (Fig. S24).[15] If the observed activation barrier for phenol transfer hydrogenation reflects the adsorption barrier for 2-propanol, the apparent activation energy should be a function of phenol concentration. Thus, Arrhenius plots were constructed to determine the variation of activation energy as a function of phenol (Fig. 5b). Indeed, at high concentrations of phenol, Pd/Ce-Na showed an apparent activation barrier of 110 kJ mol^{-1} while at low concentrations Pd/CeO_2 gave 54 kJ mol^{-1}. The transition from low to high activation barrier occurs at higher phenol concentrations for the Pd/Ce-Na catalyst. This is consistent with the Ce-Na support having more hydroxyl group binding sites than the CeO_2 support and suggests that the high activation barrier over both catalysts is due to the 2-propanol adsorption barrier in the presence of phenol. The higher amount of phenol/2-propanol adsorption and redox sites is likely related to the higher amount of O-vacancies observed from Raman studies (Fig. 2b).[46, 47, 54]

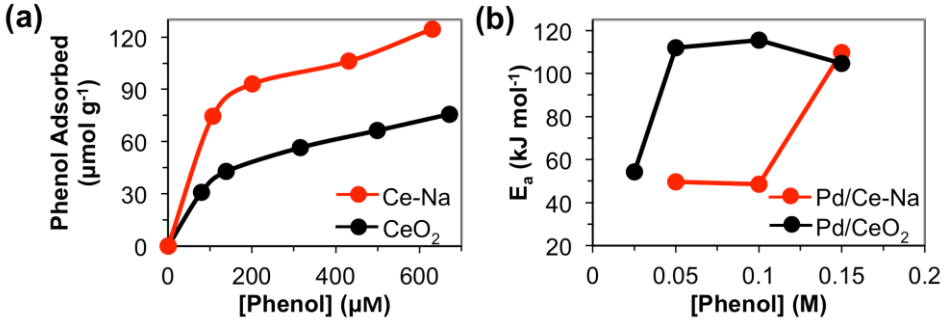

Fig. 5. (a) Phenol adsorption isotherms for Ce-Na and CeO_2. (b) Plot showing the apparent activation energy for the transfer hydrogenation of phenol as a function of phenol concentration.

3. Conclusions

The 2-propanol dehydrogenation activity of ceria is enhanced through modification with sodium by increasing the number of adsorption and redox active sites. This effect was an intrinsic property of the Ce-Na support and independent of Pd. Sodium is neither on the surface of the active material nor is it doped into ceria, but exists likely as a subsurface carbonate species of varying degrees of hydration. Deposition of palladium onto ceria and sodium-modified ceria provides catalysts active for the transfer hydrogenation of phenol using 2-propanol. The catalytic transfer hydrogenation of phenol was conducted in flow mode and required water for stability. The higher activity of the sodium-modified catalyst was attributed to the higher amount of 2-propanol/phenol adsorption sites and redox sites active for 2-propanol dehydrogenation. The apparent activation energy transitioned from low to high upon increasing phenol concentration over both catalysts and was attributed to the barrier for 2-propanol adsorption. This transition occurred at higher phenol concentrations for Pd/Ce-Na owing to the higher amount of substrate adsorption sites. Additional studies are in progress to determine the precise location of Na in the catalyst and the mechanism by which it increases the number of adsorption and redox-active sites

on ceria. Nonetheless, the enhancement of hydroxyl adsorption and redox active sites on ceria through facile sodium modification is expected to be broadly applicable to other ceria-based catalysis.

Acknowledgements

This research is supported by the U.S. Department of Energy, Office of Basic Energy Sciences, Division of Chemical Sciences, Geosciences, and Biosciences, through the Ames Laboratory Catalysis Science program. The Ames Laboratory is operated for the U.S. Department of Energy by Iowa State University under Contract No. DE-AC02-07CH11358.

Appendix A. Supplementary material

Supplementary data (Experimental, physicochemical properties of all materials, reaction data, schemes, DRIFT spectra, XPS spectra, XRD diffractograms, TEM, TGA/DSC/MS data, CO_2-TPD data, kinetic data, adsorption data) associated with this article can be found, in the online version, at

References

[1] D.L. Klass, Biomass for Renewable Energy and Fuels A2 - Cleveland, Cutler J, in: Encyclopedia of Energy, Elsevier, New York, 2004, pp. 193-212.
[2] J. Zakzeski, P.C.A. Bruijnincx, A.L. Jongerius, B.M. Weckhuysen, Chem. Rev., 110 (2010) 3552-3599.
[3] C. Xu, R.A.D. Arancon, J. Labidi, R. Luque, Chem. Soc. Rev., 43 (2014) 7485-7500.
[4] D.R. Vardon, M.A. Franden, C.W. Johnson, E.M. Karp, M.T. Guarnieri, J.G. Linger, M.J. Salm, T.J. Strathmann, G.T. Beckham, Energy Environ. Sci., 8 (2015) 617-628.
[5] M. Kleinert, T. Barth, Chem. Eng. Technol., 31 (2008) 736-745.
[6] D. Fu, S. Farag, J. Chaouki, P.G. Jessop, Bioresour. Technol., 154 (2014) 101-108.
[7] W.B. Fisher, J.F. VanPeppen, Cyclohexanol and Cyclohexanone, in: Kirk-Othmer Encyclopedia of Chemical Technology, John Wiley & Sons, Inc., 2000.

[8] H.F. Rase, Handbook of Commercial Catalysts: Heterogeneous Catalysts, CRC Press, Boca Raton, FL, 2000.
[9] J. Zhong, J. Chen, L. Chen, Catal. Sci. Technol., 4 (2014) 3555-3569.
[10] A. Chen, Y. Li, J. Chen, G. Zhao, L. Ma, Y. Yu, ChemPlusChem, 78 (2013) 1370-1378.
[11] R.D. Patil, Y. Sasson, Appl. Catal. A, 499 (2015) 227-231.
[12] D. Zhang, F. Ye, T. Xue, Y. Guan, Y.M. Wang, Catal. Today, 234 (2014) 133-138.
[13] Y. Nagasawa, H. Nanao, O. Sato, A. Yamaguchi, M. Shirai, Chem. Lett., 45 (2016) 643-645.
[14] D. Wang, D. Astruc, Chem. Rev., 115 (2015) 6621-6686.
[15] N.C. Nelson, J.S. Manzano, A.D. Sadow, S.H. Overbury, I.I. Slowing, ACS Catal., 5 (2015) 2051-2061.
[16] C. Hammond, M.T. Schümperli, S. Conrad, I. Hermans, ChemCatChem, 5 (2013) 2983-2990.
[17] L. He, J. Ni, L.-C. Wang, F.-J. Yu, Y. Cao, H.-Y. He, K.-N. Fan, Chem. Eur. J., 15 (2009) 11833-11836.
[18] M.-M. Wang, L. He, Y.-M. Liu, Y. Cao, H.-Y. He, K.-N. Fan, Green Chem., 13 (2011) 602-607.
[19] K. Shimura, K.-i. Shimizu, Green Chem., 14 (2012) 2983-2985.
[20] A. Trovarelli, Catalysis by Ceria and Related Materials, Imperial College Press, London, 2002.
[21] E. Mamontov, T. Egami, R. Brezny, M. Koranne, S. Tyagi, J. Phys. Chem. B, 104 (2000) 11110-11116.
[22] F. Esch, S. Fabris, L. Zhou, T. Montini, C. Africh, P. Fornasiero, G. Comelli, R. Rosei, Science, 309 (2005) 752-755.
[23] Y. Madier, C. Descorme, A.M. Le Govic, D. Duprez, J. Phys. Chem. B, 103 (1999) 10999-11006.
[24] S. Rossignol, F. Gerard, D. Duprez, J. Mater. Chem., 9 (1999) 1615-1620.
[25] C. Descorme, Y. Madier, D. Duprez, J. Catal., 196 (2000) 167-173.
[26] J. Guzman, S. Carrettin, A. Corma, J. Am. Chem. Soc., 127 (2005) 3286-3287.
[27] C. Li, K. Domen, K. Maruya, T. Onishi, J. Am. Chem. Soc., 111 (1989) 7683-7687.
[28] V.V. Pushkarev, V.I. Kovalchuk, J.L. d'Itri, J. Phys. Chem. B, 108 (2004) 5341-5348.
[29] R.J. Gorte, AIChE J., 56 (2010) 1126-1135.
[30] J.A. Rodriguez, X. Wang, P. Liu, W. Wen, J.C. Hanson, J. Hrbek, M. Pérez, J. Evans, Top. Catal., 44 (2007) 73-81.
[31] A. Trovarelli, Catal. Rev., 38 (1996) 439-520.
[32] J. Paier, C. Penschke, J. Sauer, Chem. Rev., 113 (2013) 3949-3985.
[33] B. Murugan, A.V. Ramaswamy, J. Am. Chem. Soc., 129 (2007) 3062-3063.
[34] N.J. Lawrence, J.R. Brewer, L. Wang, T.S. Wu, J. Wells-Kingsbury, M.M. Ihrig, G. Wang, Y.L. Soo, W.N. Mei, C.L. Cheung, Nano Lett, 11 (2011) 2666-2671.
[35] X. Liu, K. Zhou, L. Wang, B. Wang, Y. Li, J. Am. Chem. Soc., 131 (2009) 3140-3141.
[36] D.-Z. Peng, S.-Y. Chen, C.-L. Chen, A. Gloter, F.-T. Huang, C.-L. Dong, T.-S. Chan, J.-M. Chen, J.-F. Lee, H.-J. Lin, C.-T. Chen, Y.-Y. Chen, Langmuir, 30 (2014) 10430-10439.
[37] L. Chen, P. Fleming, V. Morris, J.D. Holmes, M.A. Morris, J. Phys. Chem. C, 114 (2010) 12909-12919.
[38] S.D. Senanayake, D. Stacchiola, J.A. Rodriguez, Acc. Chem. Res., 46 (2013) 1702-1711.
[39] Y. Lin, Z. Wu, J. Wen, K.R. Poeppelmeier, L.D. Marks, Nano Lett, 14 (2014) 191-196.

583 [40] H.-X. Mai, L.-D. Sun, Y.-W. Zhang, R. Si, W. Feng, H.-P. Zhang, H.-C. Liu, C.-H. Yan, J.
584 Phys. Chem. B, 109 (2005) 24380-24385.
585 [41] Z. Wu, M. Li, J. Howe, H.M. Meyer, S.H. Overbury, Langmuir, 26 (2010) 16595-16606.
586 [42] Z. Wu, M. Li, S.H. Overbury, J. Catal., 285 (2012) 61-73.
587 [43] E. Aneggi, D. Wiater, C. de Leitenburg, J. Llorca, A. Trovarelli, ACS Catal., 4 (2014) 172-
588 181.
589 [44] Z. Wu, M. Li, D.R. Mullins, S.H. Overbury, ACS Catal., 2 (2012) 2224-2234.
590 [45] M. Li, Z. Wu, S.H. Overbury, J. Catal., 306 (2013) 164-176.
591 [46] R.M. Ferrizz, G.S. Wong, T. Egami, J.M. Vohs, Langmuir, 17 (2001) 2464-2470.
592 [47] D.R. Mullins, M.D. Robbins, J. Zhou, Surf. Sci., 600 (2006) 1547-1558.
593 [48] A. Siokou, R.M. Nix, J. Phys. Chem. B, 103 (1999) 6984-6997.
594 [49] J.P. Torella, C.J. Gagliardi, J.S. Chen, D.K. Bediako, B. Colón, J.C. Way, P.A. Silver, D.G.
595 Nocera, Proc. Natl. Acad. Sci. U.S.A, 112 (2015) 2337-2342.
596 [50] L. Vaccaro, D. Lanari, A. Marrocchi, G. Strappaveccia, Green Chem., 16 (2014) 3680-3704.
597 [51] F.-t. Li, J. Ran, M. Jaroniec, S.Z. Qiao, Nanoscale, 7 (2015) 17590-17610.
598 [52] D.R. Mullins, S.D. Senanayake, T.L. Chen, J. Phys. Chem. C, 114 (2010) 17112-17119.
599 [53] D.R. Mullins, P.M. Albrecht, F. Calaza, Top. Catal., 56 (2013) 1345-1362.
600 [54] D.R. Mullins, Surf. Sci. Rep., 70 (2015) 42-85.
601 [55] D.R. Mullins, P.M. Albrecht, T.-L. Chen, F.C. Calaza, M.D. Biegalski, H.M. Christen, S.H.
602 Overbury, J. Phys. Chem. C, 116 (2012) 19419-19428.
603 [56] B. Chen, Y. Ma, L. Ding, L. Xu, Z. Wu, Q. Yuan, W. Huang, J. Phys. Chem. C, 117 (2013)
604 5800-5810.
605 [57] M. Molinari, S.C. Parker, D.C. Sayle, M.S. Islam, J. Phys. Chem. C, 116 (2012) 7073-7082.
606 [58] M. Yang, J. Liu, S. Lee, B. Zugic, J. Huang, L.F. Allard, M. Flytzani-Stephanopoulos, J.
607 Am. Chem. Soc., 137 (2015) 3470-3473.
608 [59] Y. Zhai, D. Pierre, R. Si, W. Deng, P. Ferrin, A.U. Nilekar, G. Peng, J.A. Herron, D.C. Bell,
609 H. Saltsburg, M. Mavrikakis, M. Flytzani-Stephanopoulos, Science, 329 (2010) 1633-1636.
610 [60] R. Shannon, Acta Crystallogr. Sect. A, 32 (1976) 751-767.
611 [61] M.-F. Luo, Z.-L. Yan, L.-Y. Jin, M. He, J. Phys. Chem. B, 110 (2006) 13068-13071.
612 [62] J.R. McBride, K.C. Hass, B.D. Poindexter, W.H. Weber, J. Appl. Phys., 76 (1994) 2435-
613 2441.
614 [63] T. Taniguchi, T. Watanabe, N. Sugiyama, A.K. Subramani, H. Wagata, N. Matsushita, M.
615 Yoshimura, J. Phys. Chem. C, 113 (2009) 19789-19793.
616 [64] J.E. Spanier, R.D. Robinson, F. Zhang, S.-W. Chan, I.P. Herman, Phys. Rev. B, 64 (2001)
617 245407.
618 [65] M. Li, U. Tumuluri, Z. Wu, S. Dai, ChemSusChem, 8 (2015) 3651-3660.
619 [66] R.V. Siriwardane, J.A. Poston, C. Robinson, T. Simonyi, Energy Fuels, 25 (2011) 1284-
620 1293.
621 [67] J.S. Hammond, J.W. Holubka, J.E. deVries, R.A. Dickie, Corros. Sci., 21 (1981) 239-253.
622 [68] H.S. Dunsmore, J.C. Speakman, Acta Crystallogr., 16 (1963) 573-574.
623 [69] M. Dusek, G. Chapuis, M. Meyer, V. Petricek, Acta Crystallogr. Sect. B, 59 (2003) 337-
624 352.
625 [70] A. Pfau, K.D. Schierbaum, Surf. Sci., 321 (1994) 71-80.
626 [71] M. Romeo, K. Bak, J. El Fallah, F. Le Normand, L. Hilaire, Surf. Interface Anal., 20 (1993)
627 508-512.
628 [72] C. Hardacre, G.M. Roe, R.M. Lambert, Surf. Sci., 326 (1995) 1-10.

[73] S.D. Senanayake, D.R. Mullins, J. Phys. Chem. C, 112 (2008) 9744-9752.
[74] L. Chen, J. Zhao, S.-F. Yin, C.-T. Au, RSC Adv., 3 (2013) 3799-3814.
[75] H. Hattori, Chem. Rev., 95 (1995) 537-558.
[76] H.N. Evin, G. Jacobs, J. Ruiz-Martinez, U.M. Graham, A. Dozier, G. Thomas, B.H. Davis, Catal. Lett., 122 (2008) 9-19.
[77] N.J. Lawrence, J.R. Brewer, L. Wang, T.-S. Wu, J. Wells-Kingsbury, M.M. Ihrig, G. Wang, Y.-L. Soo, W.-N. Mei, C.L. Cheung, Nano Lett., 11 (2011) 2666-2671.
[78] M.I. Zaki, N. Sheppard, J. Catal., 80 (1983) 114-122.
[79] K.S. Mazdiyasni, L.M. Brown, Inorg. Chem., 9 (1970) 2783-2786.
[80] M.I. Zaki, G.A.M. Hussein, H.A. El-Ammawy, S.A.A. Mansour, J. Polz, H. Knözinger, J. Molec. Catal., 57 (1990) 367-378.
[81] P.A. Redhead, Vacuum, 12 (1962) 203-211.
[82] R. Masel, Principles of Adsorption and Reaction on Solid Surfaces, Wiley-Interscience, 1996.
[83] J.L. Davis, M.A. Barteau, Surf. Sci., 187 (1987) 387-406.

Graphical abstract

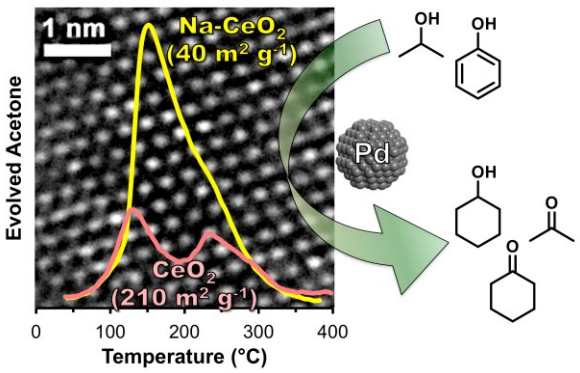

Highlights

- Liquid flow transfer hydrogenation of phenol performed over Pd/CeO_2 and Pd/Ce-Na.
- Pd/Ce-Na shows 6x higher activity than Pd/CeO_2.
- Water-stable sodium species seemingly exist as subsurface carbonate spectators.
- Na-modification increases the number of substrate adsorption and redox active sites
- High apparent activation energies reflect propanol adsorption barrier in presence of phenol.

656 **List of tables**

661

662 **Table 1.** Reaction conditions and catalytic results for transfer hydrogenation of phenol with 2-
663 propanol.[a]

Entry	Catalyst	Phenol (M)	Flow Rate (μL min^{-1})	Conversion Rate (μmol g^{-1} h^{-1})	Yield (%)		K:A
					C=O	C-OH	
1	Pd/Ce-Na	0.150	44.1[b]	759 ± 6	13 ± 1	82 ± 1	14:86
2	Pd/Ce-Na	0.150	95.6[c]	1390 ± 40	26 ± 1	54 ± 2	33:67
3	Pd/Ce-Na	0.150	191[d]	1410 ± 20	16 ± 1	25 ± 1	40:60
4	Pd/Ce-Na	0.200	44.1	905 ± 16	19 ± 1	67 ± 2	22:78
5	Pd/Ce-Na	0.200	95.6	1360 ± 60	18 ± 1	41 ± 3	30:70
6	Pd/CeO_2	0.150	44.1	266 ± 9	31 ± 4	2 ± 1	93:7
7	Pd/CeO_2	0.150	95.6	287 ± 8	16 ± 1	<1	96:4
8	Pd/CeO_2	0.150	191	279 ± 3	8 ± 1	0	100:0
9	Pd/CeO_2	0.200	44.1	215 ± 4	20 ± 2	<1	97:3
10	Pd/CeO_2	0.200	95.6	217 ± 5	10 ± 2	0	100:0

664 [a]0.5g of catalyst was used for all reactions. Water was flowed over the catalyst at room
665 temperature for 2 h before beginning the initial run (Entries 1, 6). After that, the reactions were
666 run sequentially (Entries 2-5, 7-10). 90 v/v % aqueous 2-propanol was used for all reactions.
667 Column temperature was 140 °C. Catalyst bed volume (V_{bed}) was 0.4 mL. Errors are reported as
668 one standard deviation away from the mean. [b]For a flow rate of ~0.05 mL min^{-1}, 72 mL of
669 reagent was used with 12 mL sample composite intervals generating 6 data points over 24 h. [c]For
670 a flow rate of ~0.10 mL min^{-1}, 144 mL of reagent was used with 24 mL sample composite
671 intervals generating 6 data points over 24 h. [d]For a flow rate of ~0.20 mL min^{-1}, 168 mL of
672 reagent was used with 24 mL sample composite intervals generating 7 data points over 14 h.

673

Table 2. Physicochemical properties of supports and catalysts under varying conditions.

Entry	Sample	Surface Area (m^2 g^{-1})[a]	Na Loading (at. %)[b]	Lattice Constant (Å)[c]
1	Ce-Na	29	18 ± 1[d]	5.412
2	CeO_2	210	0	5.412
3	Ce-Na[e]	42	4.0 ± 0.2[f]	5.412
4	Ce-Na[g]	40	2.6 ± 0.1[h]	---
5	Pd/Ce-Na[i]	20	2.7 ± 0.2[j]	---

[a]Determined by nitrogen physisorption using BET approximation. [b]Determined by ICP-OES and is relative to Ce. [c]Determined using HighScore software. [d]Measured across three batches. [e]Washed with flowing water (0.1 mL min^{-1}) for 12 h at room temperature. [f]Measured across two batches with two sample preps in duplicate (i.e. 8 data points). [g]Washed with flowing water (0.1 mL min^{-1}) for 12 h at 140 °C. [h]Measured for one batch with two sample preparations in duplicate (i.e. 4 data points). [i]Results after 7 d reaction. [j]Measured in duplicate with two sample preparations (i.e. 4 data points).

685 **Table 3.** Acetone formation rates over supports and catalysts in absence and presence of phenol.[a]

Entry	Catalyst	[Phenol] (M)	Acetone Rate (μmol g^{-1} h^{-1})	C=O Rate (μmol g^{-1} h^{-1})[b]	C-OH Rate (μmol g^{-1} h^{-1})[b]	Expected Acetone Rate (μmol g^{-1} h^{-1})[c]
1	CeO_2	0	7 ± 0.7[e]	---	---	---
2	Ce-Na	0	13 ± 1.3[e]	---	---	---
3	Pd/CeO_2	0	2920 ± 80[d]	---	---	---
4	Pd/Ce-Na	0	6270 ± 40[d]	---	---	---
5	Pd/CeO_2	0.15	576 ± 58[e]	288	12	612
6	Pd/Ce-Na	0.15	3680 ± 368[e]	476	974	3874

686 [a]Conditions: 90 v/v % aqueous 2-propanol, 0.5g of catalyst, 0.1 mL min^{-1}, T = 140 °C, V_{bed} =
687 0.4 mL. [b]Rates obtained from data found in Table 1, Entries 2, 7. [c]Calculated assuming 2 moles
688 of acetone per mole of cyclohexanone and 3 moles of acetone per mole of cyclohexanol.
689 [d]Average rate from three separate reactions. Errors represent one standard deviation from the
690 mean. [e]Rate from one reaction. Errors represent average relative error determined during method
691 validation (see experimental).

692

693

List of figures

Fig. 1. (a) Phenol conversion rate for Pd/CeO_2 and Pd/Ce-Na during 7 day time-on-stream (TOS) study. Conditions: 0.15 M phenol in 90 v/v % aqueous 2-propanol, 0.5 g catalyst, ~0.1 mL min^{-1}, T = 140 °C, V_{bed} = 0.4 mL. Each data point corresponds to 72 mL product stream composite. (b) Arrhenius plots of phenol conversion over Pd/CeO_2 (E_A = 115 kJ mol^{-1}) and Pd/Ce-Na (E_A = 48 kJ mol^{-1}). Conditions: 0.1 M phenol in 90 v/v % aqueous 2-propanol, 0.5 g catalyst, ~0.1 mL min^{-1}, V_{bed} = 0.4 mL. Each data point (at each temperature) corresponds to the average of 6 rate measurements collected at 4 h sampling intervals (24 mL composite) over 24 h.

Fig. 2. (a) PXRD patterns for CeO_2 and Ce-Na showing cubic fluorite phase. (b) Raman spectra using 488 nm excitation for CeO_2 and Ce-Na. Inset shows band associated with intrinsic defects (D-band). The numbers represent the ratio (A_D:A_{F2g}) of the peak areas for the D-band (600 cm^{-1}) and the F_{2g}-band (462 cm^{-1}).

Fig. 3. TPD-MS profile for TPSR of adsorbed 2-propanol on (a) CeO_2 and (b) Ce-Na. The m/z =41, 43, and 45 signals correspond to propylene, acetone, and 2-propanol, respectively. Mass normalized TPD-MS profile for TPSR of adsorbed 2-propanol on Ce-Na and CeO_2 while monitoring (c) m/z = 58 and (d) m/z = 45 which correspond to acetone and 2-propanol, respectively.

Fig. 4. Phenol conversion rate versus phenol concentration over Pd/CeO_2 and Pd/Ce-Na. Conditions: 90 v/v % aqueous 2-propanol, 0.5 g catalyst, ~0.1 mL min^{-1}, T = 140 °C, V_{bed} = 0.4 mL.

Fig. 5. (a) Phenol adsorption isotherms for Ce-Na and CeO_2. (b) Plot showing the apparent activation energy for the transfer hydrogenation of phenol as a function of phenol concentration.

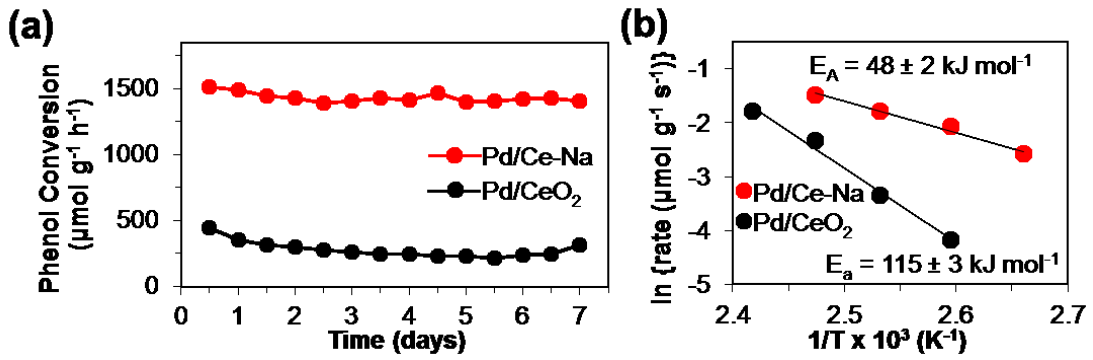

716

717 **Fig. 1.** (a) Phenol conversion rate for Pd/CeO_2 and Pd/Ce-Na during 7 day time-on-stream (TOS)
718 study. Conditions: 0.15 M phenol in 90 v/v % aqueous 2-propanol, 0.5 g catalyst, ~0.1 mL min^{-1},
719 T = 140 °C, V_{bed} = 0.4 mL. Each data point corresponds to 72 mL product stream composite. (b)
720 Arrhenius plots of phenol conversion over Pd/CeO_2 (E_A = 115 kJ mol^{-1}) and Pd/Ce-Na (E_A = 48
721 kJ mol^{-1}). Conditions: 0.1 M phenol in 90 v/v % aqueous 2-propanol, 0.5 g catalyst, ~0.1 mL
722 min^{-1}, V_{bed} = 0.4 mL. Each data point (at each temperature) corresponds to the average of 6 rate
723 measurements collected at 4 h sampling intervals (24 mL composite) over 24 h.

724

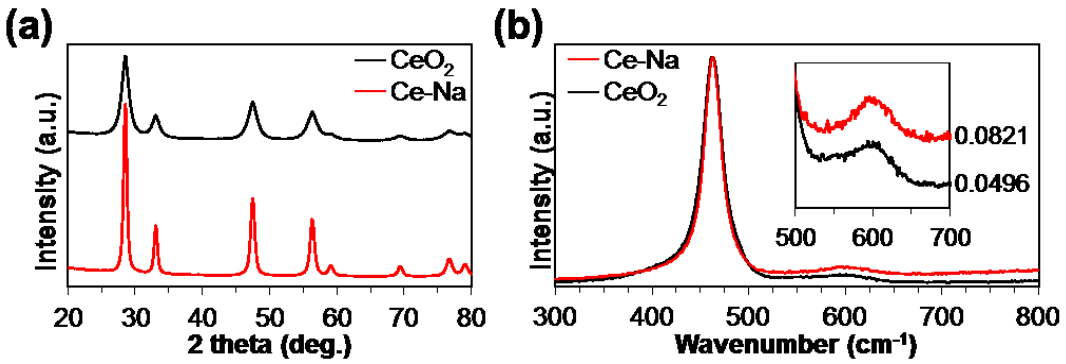

725

726 **Fig. 2.** (a) PXRD patterns for CeO_2 and Ce-Na showing cubic fluorite phase. (b) Raman spectra
727 using 488 nm excitation for CeO_2 and Ce-Na. Inset shows band associated with intrinsic defects
728 (D-band). The numbers represent the ratio (A_D:A_{F2g}) of the peak areas for the D-band (600 cm^{-1})
729 and the F_{2g}-band (462 cm^{-1}).

730

731

732

733

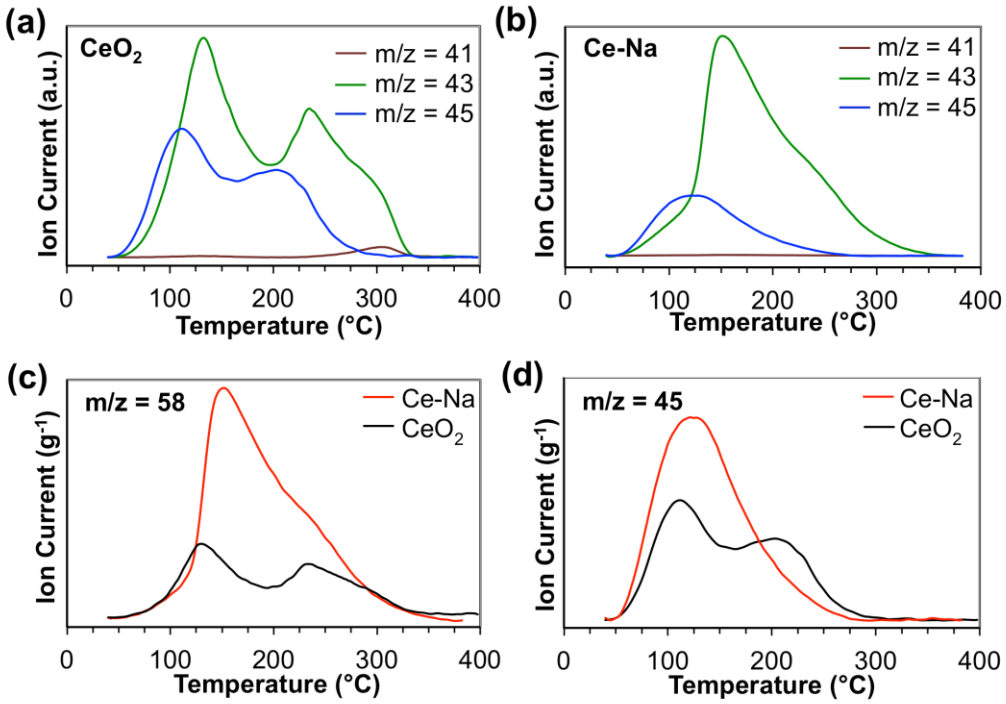

734

735 **Fig. 3.** TPD-MS profile for TPSR of adsorbed 2-propanol on (a) CeO_2 and (b) Ce-Na. The m/z
736 =41, 43, and 45 signals correspond to propylene, acetone, and 2-propanol, respectively. Mass
737 normalized TPD-MS profile for TPSR of adsorbed 2-propanol on Ce-Na and CeO_2 while
738 monitoring (c) m/z = 58 and (d) m/z = 45 which correspond to acetone and 2-propanol,
739 respectively.

740

741

742

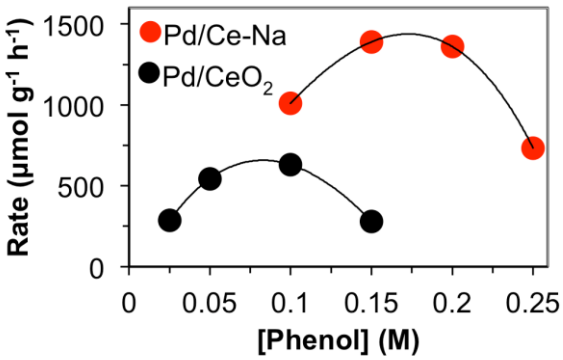

743

744 **Fig. 4.** Phenol conversion rate versus phenol concentration over Pd/CeO_2 and Pd/Ce-Na.

745 Conditions: 90 v/v % aqueous 2-propanol, 0.5 g catalyst, ~0.1 mL min^{-1}, T = 140 °C, V_{bed} = 0.4

746 mL.

747

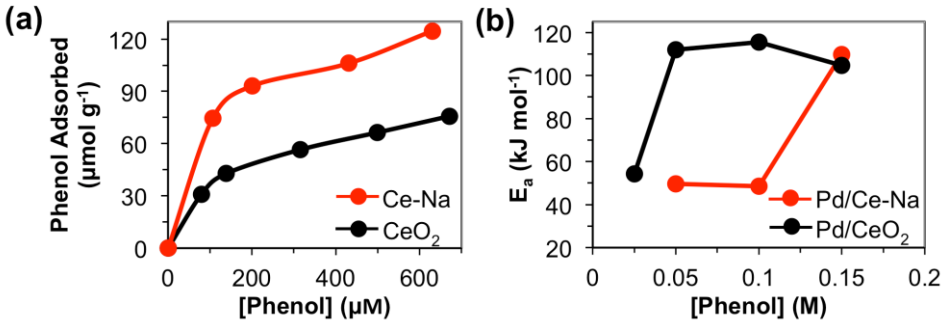

748

749 **Fig. 5.** (a) Phenol adsorption isotherms for Ce-Na and CeO_2. (b) Plot showing the apparent

750 activation energy for the transfer hydrogenation of phenol as a function of phenol concentration.

751